



Soft Matter

On the blistering of thermo-sensitive hydrogel: the volume phase transition and mechanical instability

Journal:	<i>Soft Matter</i>
Manuscript ID	SM-ART-05-2019-000911.R2
Article Type:	Paper
Date Submitted by the Author:	25-Jun-2019
Complete List of Authors:	Shen, Tong; University of Colorado Boulder, Mechanical Engineering Kan, Jian; University of Colorado Boulder, Mechanical Engineering Benet, Eduard; University of Colorado Boulder, Mechanical Engineering Vernerey, Franck; University of Colorado at Boulder, Department of Mechanical Engineering; University of Colorado Boulder

SCHOLARONE™
Manuscripts

Cite this: DOI: 10.1039/xxxxxxxxxx

On the blistering of thermo-sensitive hydrogel: the volume phase transition and mechanical instability[†]

Tong Shen, Jian Kan, Eduard Benet and Franck J. Vernerey,*

Received Date
Accepted Date

DOI: 10.1039/xxxxxxxxxx

www.rsc.org/journalname

This paper explores the physical mechanisms responsible for the appearance of small blisters on the surface of temperature sensitive hydrogels as they deswell rapidly during their volume phase transition. For this, we develop a numerical model that couples the processes of hydrogel deswelling and blister growth due to the existence of a thin quasi-impermeable layer on its surface. The model points out that blister inflation originates at defects point under the gel's surface, under the effect of the increasing osmotic pressure in the gel as it undergoes its phase transition. Due to their large deformation, these blisters often experience a mechanical instability that triggers a sudden increase in their growth rate at the expense of their closest neighbors. Using a simple computational model, we then show that blisters are able to communicate via internal pressure and that these interactions are mediated by two characteristic time scales related to solvent transport within and between adjacent blisters. Our study finally indicates that these mechanisms can be controlled by temperature and the gel's cross-link density to achieve diversity of blister patterns on the gel's surface. The proposed analysis provides predictions that agree well with experimental observations of NiPAm gels which deswell in various conditions.

1 INTRODUCTION

Blistering is a common mode of failure in materials composed of a thin and flexible film adhered to a solid substrate. Typically, a mismatch between bulk and film deformation, or the infiltration of an interstitial fluid between the two materials creates their delamination and the appearance of bulges that can take a variety of shapes and sizes.¹ Practically, blisters are therefore often associated with skin damage from forceful rubbing, burning or chemical exposure.² They are also commonly observed in paint, film coatings,³ as well as composite materials.⁴ Blisters, are also used by living cells when they trigger the detachment of the plasma membrane from the stiffer underlying cortex.⁵ In this situation, the resulting "blebs" enable biological functions that are critical in the processes of apoptosis,⁵ locomotion,^{6,7} and cytokinesis.⁸

The formation of blister does not always require the presence of a surface film. For instance, heat-stimulus hydrogels, such as poly(N-isopropylacrylamide) (PNIPAm), exhibit a variety of blister-like protrusions on their surface as they transit from their swollen to unswollen phase.⁹ The occurrence of these bubble-like

patterns has indeed been observed as the gel quickly shrinks at the lower critical solution temperature $LCST = 32^{\circ}C$ ¹⁰ with shapes and sizes that are sensitive to shrinking rate.^{11,12} Harnessing this phenomenon may have interesting applications in drug delivery,^{13,14} soft robotics,^{15–17} and microfluidic devices.^{18,19} For this reason, a number of studies have been undertaken to better understand the physical mechanisms responsible for hydrogel blistering. In this context, Matsuo and Tanaka²⁰ reported a variety of pattern formation in Acrylamide hydrogels immersed in acetone solution. They further suggested that surface blisters start with the formation of a dense, impermeable layer on the gel's surface in the early stage of shrinking. As a consequence, water is restricted to the gel core in spite of being a bad solvent. Under this volume constraint, a competition takes place between areas undergoing shrinking and those being filled with the trapped fluid. Eventually, this mechanism leads to a phase-separation between swollen and unswollen gel with the associated blister-like patterns. To validate this hypothesis, further experiments were performed on thermo-sensitive PNIPAm hydrogel wherein gels were subjected to a variety of heating rates to control the speed of their swollen-to-unswollen phase transition. Results indicate that for low heating rates ($< 0.033^{\circ}Cmin^{-1}$), a gel surface pattern take the form of peristaltic patterns that clearly show the phase coexistence predicted by theoretical considerations. By contrast, higher heating rates are associated with bubble-shape patterns^{21,22} whose formation mechanism

^a University of Colorado Boulder, Boulder, CO, USA, 80302; E-mail: Franck.Vernerey@colorado.edu

[†] Electronic Supplementary Information (ESI) available: [details of any supplementary information available should be included here]. See DOI: 10.1039/b000000x/

is still subject to debate for the following reasons. First, unlike the peristaltic patterns that show longitudinal periodicity, bubble patterns are distributed randomly on the gel surface while its bulk remains homogeneous.²³ Second, gels with higher inhomogeneity in their network, which is considered to favor the phase separation, exhibit fewer patterns during shrinking.^{24–26} This suggests that although phase separation occurs in the early stage of shrinking, it is not the reason for the formation of bubbles.¹¹ Instead, it is believed that the gel forms an impermeable layer on its surface which delaminates and form spherical blisters when its internal pressure becomes sufficiently large. This scenario suggests that the patterns are actual water-filled blisters rather than a swollen gel. This hypothetical mechanism was backed up by Tokita et al.^{27,28} who used confocal microscopy to observe the formation of the skin layer and the resulting water-filled blisters. Shibayama²⁹ further reported that the formation of these blisters were affected by the gel's crosslink density; wherein a lower crosslink density promoted the formation of blisters. Kaneko et al.³⁰ performed multiple shrinking-swelling cycles and found that gels that had undergone one or several cycles formed smaller blisters. This is likely caused by the accumulation of damage on early cycles promoting water leak through the gel surface, instead of accumulating in blisters.

Despite these experimental efforts, the mechanics of blister is still not fully understood and has not been the object of theoretical studies.³¹ To address this shortcoming, we have explored the mechanics blister formation and its related patterns in thermosensitive PNIPAM hydrogels from a modeling perspective. We first study how a blister is formed on the skin layer of the gel and identify the key factors that determine its size and shape. We then investigate the competition between multiple interacting blisters and identify the key mechanisms that regulate the hydrogel surface profile. This understanding leads to a two-dimensional simplified model that qualitatively explain experimental findings regarding the blister growth on the hydrogel surface.

2 DESWELLING AND SURFACE BLISTERING OF PNIPAM HYDROGELS

As discussed above, thermosensitive PNIPAM hydrogels are well known for their capability to undergo a sharp volume phase transition around the lower critical swelling temperature (LCST) of 32°C.³² When the temperature quickly rises around the LCST, hydrogel deswelling can occur in a highly heterogeneous manner as seen in Fig.1a. We here discuss an experimental approach to characterize and quantify this phenomenon, and further propose the most probable physical mechanisms at play based on our observations.

2.1 Experimental observation of surface blistering

To characterize the inhomogeneous deswelling of PNIPAM hydrogels, we fabricated cylindrical specimens using the radical polymerization technique³³ and placed them in water bath of temperature $T=320$ K. Fig.1a shows the sequential deformation

of a specimen, originally in its swollen state at $T = 293$ K (with a diameter of 1 cm and a length of 5 cm) as it is suddenly dipped into a hot water bath. During deswelling, the gel exhibits the temporary appearance of large surface blisters that induce a strong gel distortion. Our observations indicate that the shrinking process goes through four distinct stages. Stage i (①-②) is characterized by a uniform shrinking, i.e., the specimen remains cylindrical until approximately 90% of its initial diameter is reached. In stage ii, or "plateau stage",¹¹ the shrinking process stalls for a small period (②-③) before blisters start to appear on the gel's surface at time ③. At this point, the deswelling process enters a third stage (stage iii) characterized by a high shrinking rate and the fast growth of multiple blisters on the gel's surface. We note that gel bending may also be observed due to the asymmetric growth of the blisters on opposite sides. The last stage (stage iv) is finally associated with the slow deflation of the blisters until the gel recovers its cylindrical unswollen shape at time ⑤. The duration of this stage is usually 3 to 4 times that of the first three stages combined.

To further characterize the dependency of this phenomenon on experimental parameters, hydrogels with different crosslink densities ($\rho = 0.54\rho_0, 1.0\rho_0, 1.58\rho_0$ and $2.23\rho_0$ where $\rho_0 = 103.02$ M/m³) were dipped into water baths at three different temperatures $T = 310$ K, 320 K and 330 K. The surface profiles of the gels were characterized at time ④ shown in Fig. 1a when the shrinking of the gel stalls. To quantify the phenomenon, we evaluated the surface density of blisters by n/A_0 where n is the total number of blisters and A_0 is the initial surface area of the gel (see Supplemental Information for more detail on the measurements of crosslink density and blister density). Interestingly, we find that blister density scales linearly with both temperature and crosslink density (Fig. 1c). We observed that decreasing the crosslink density or increasing the bath temperature led to a higher blister density (Fig. 1b and c). For high crosslink density ($\rho = 2.23\rho_0$), the surface blistering was fully hindered. In addition, Fig. 1c visually shows that the average size of blisters becomes smaller for a higher blister density. Although most blisters take a sphere-like shape, non-axisymmetric blisters are also seen in image H and I. This could be caused by the local heterogeneities in gel's properties, and the non-uniform curvature of the gel's surface. Due to these irregular shapes, an accurate measurement of their average size was challenging to obtain via image processing, preventing a quantitative measurement of this quantity.

To explore the mechanism behind these observations, we placed cylindrical PNIPAM specimens in water baths of different temperatures ranging from 293 K to 325 K for 6 hours and allowed them to reach the swelling equilibrium. In the context of blister growth, a useful measure of the volume phase transition is provided by the reduced volume $V^* = (1 - V/V_s)$ where V is current volume of the gel and V_s is the swollen volume of gel at $T = 293$ K. This quantity indeed quantifies the relative loss of water in the gel compared to its swollen state. Experimental results shown in Fig. 2a indicate that PNIPAM hydrogels process two distinct phases across the temperature range, most notably between

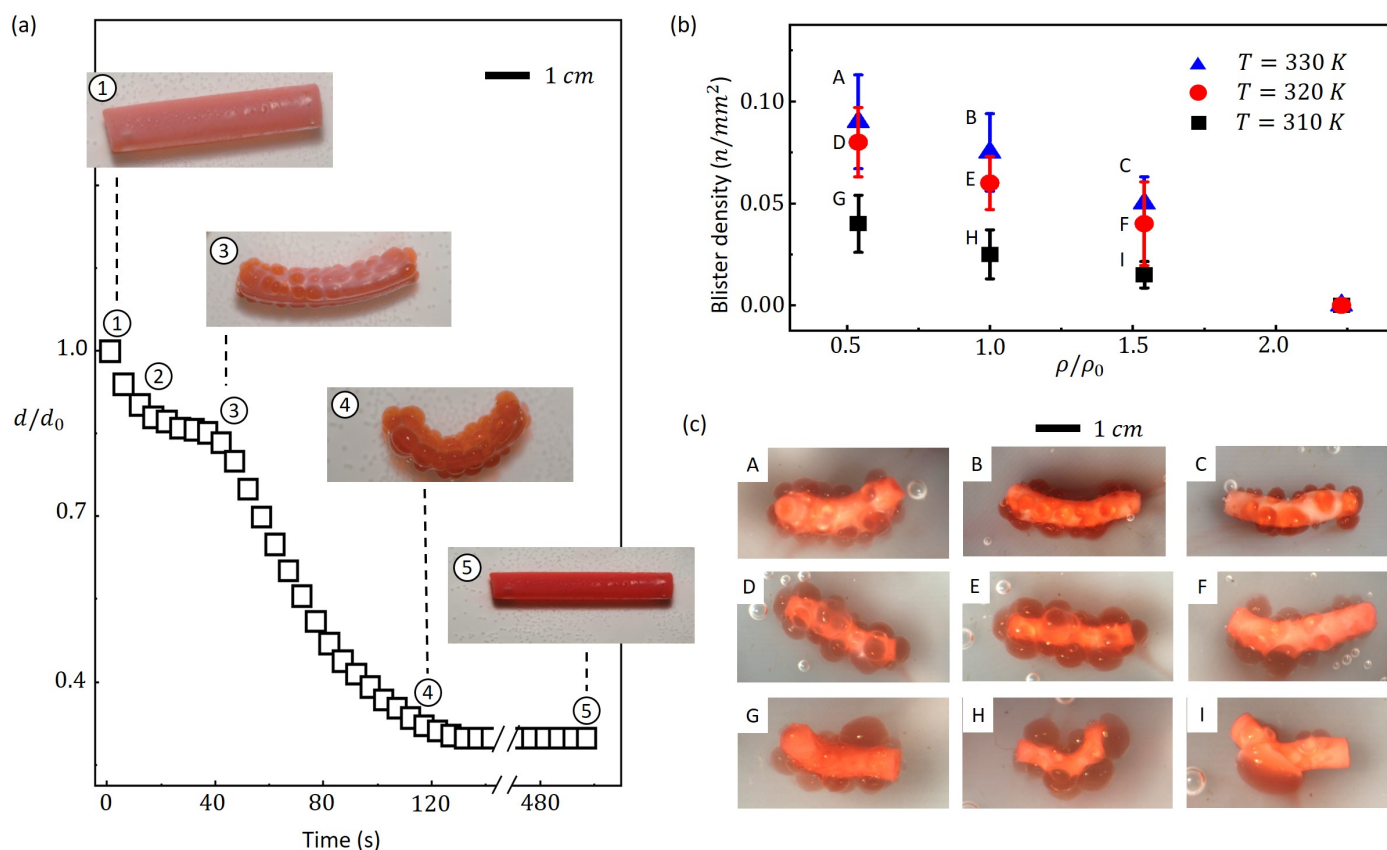


Fig. 1 (a) The decrease in diameter of a hydrogel as a function of time when it is dipped in a hot water bath of 320 K. The inset shows the morphology of the gel at different times. (b) Dependency of blister density on crosslink density and temperature. Data points are obtained by averaging 3 repeats for each condition. (c) Experimental image about the surface profile of hydrogels for different experimental conditions. Images are taken when the hydrogel core stops shrinking (time ⑤).

300 K and 310 K. The origin of this separation can be explained by the interplay between two competing forces: the polymer-solvent mixing force and the elasticity of the cross-linked polymer network. Gel swelling arises from the affinity between solvent and polymer and is balanced by the stretching resistance of the cross-linked chain network. The Flory-Rhener theory³⁴ has been successful at predicting this competition by decomposing the gel's Gibb's free energy ΔG into a mixing (ΔG^{mix}) and an elastic (ΔG^{el}) contribution, such that $\Delta G(J, \chi) = \Delta G^{mix}(J, \chi) + \Delta G^{el}(J)$ where J denotes the swelling ratio. The Flory-Huggins parameter χ measures the affinity between polymer and solvent (a smaller value of χ indicates a greater affinity³⁵). Using this theoretical framework and assuming that the polymer network is a neo-Hookean hyperelastic material,³⁶ it can be shown (see Supplemental Information) that the equilibrium hydrostatic pressure $P_g = 3(\partial \Delta G / \partial J)$ is split into an elastic (P_e) and an osmotic (π) contribution as follows:

$$P_g = P_e + \pi \quad \text{where} \quad P_e = E(J^{-1/3} - J^{-1})$$

$$\text{and} \quad \pi = \frac{k_B T}{v} \left[\ln(1 - J^{-1}) + J^{-1} + \chi J^{-2} \right] \quad (1)$$

In the above equations, $E = 3\rho k_B T$ is the polymer's Young's modulus, ρ is the crosslink density in the dry state, $k_B T$ is the thermal energy and v is the solvent's specific volume. The equilibrium

state is achieved when the osmotic and elastic pressures are balanced (i.e., $P_g = 0$) for a given reduced volume V^* , as shown in Fig. 2b. We note that the V^* and J are related by the relation $V^* = 1 - J/J_s$ where J_s is the swelling ratio at room temperature 298 K. The extreme temperature sensitivity of PNIPAm between 300 K and 310 K is due to the temperature dependence of the interaction parameter χ as characterized by Afroze et al.³² using a series of polynomial. In this study, we take the first order approximation. Note that this approximation is sufficient for evaluating the swelling ratio except at the LCST. At the LCST, the equilibrium state is unstable and requires higher order approximation, as pointed by Cai and Suo³⁷. Since this unstable equilibrium is beyond the scope of this study, we only take the first order term as $\chi = \chi_0 + \chi_1 T$ where $\chi_0 = -12.917$ and $\chi_1 = 0.044959 K^{-1}$ are calibrated parameters. We show in Fig. 2b that changes in χ drastically switch the swelling equilibrium of the gel from $V^* \approx 0.06$ at $T = 300$ K ($\chi = 0.51$) to $V^* = 0.93$ at $T = 310$ K ($\chi = 0.92$). This yields a volume reduction by more than 10-folds across this temperature range. Once this transition has occurred, further heating does not significantly affect the gel's volume, which settles around a reduced volume $V^* \approx 0.98$.

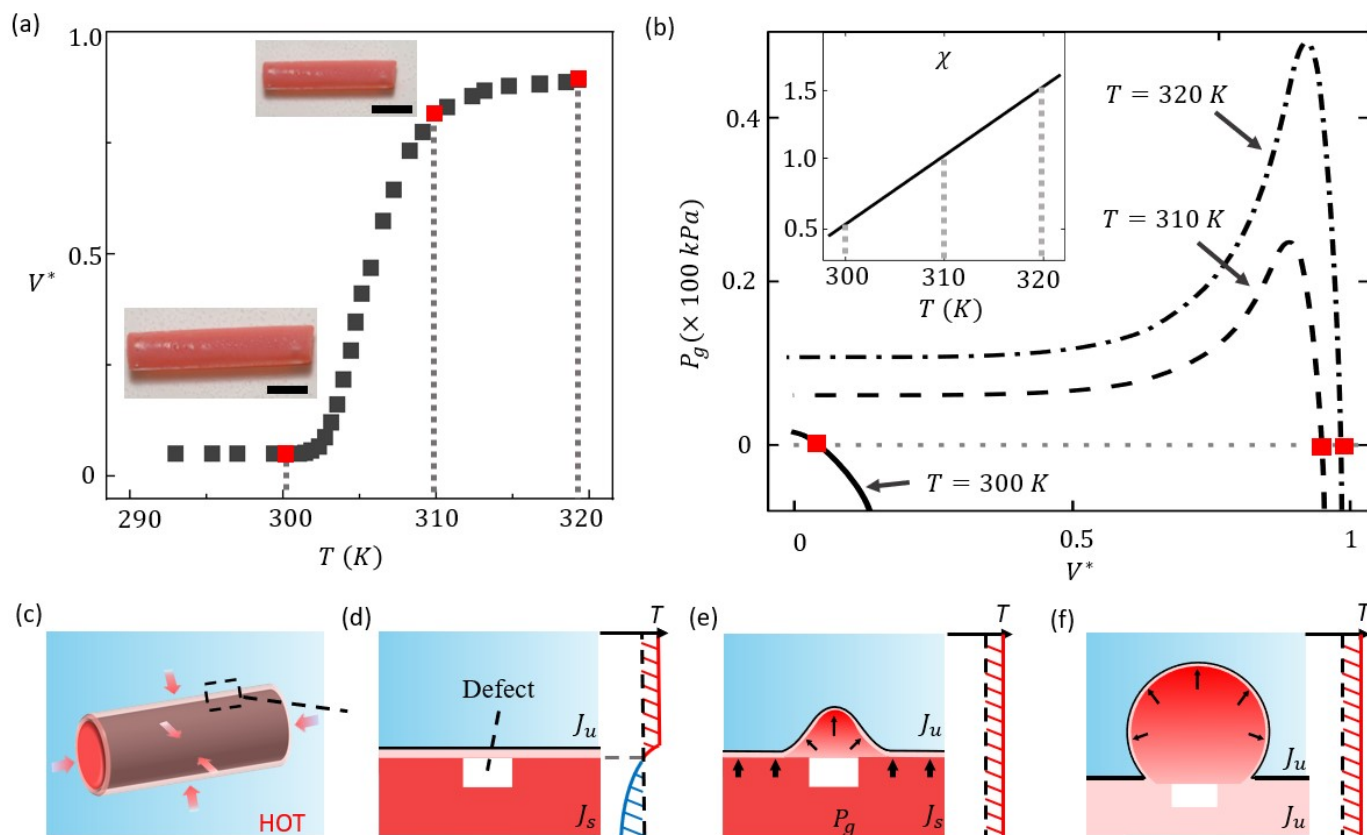


Fig. 2 (a) Swelling ratio of NIPAM hydrogel as a function of temperature. The scale bar represents 1 cm (b) Curves of hydrogel pressure P_g as a function of reduced volume V^* . The inset shows the dependency of the interaction parameter χ on temperature. (c)–(f) Schematic illustration of the mechanisms behind surface blistering during hydrogel deswelling

2.2 Shrinking process and blister formation

To explain the appearance of blisters on the gel surface during gel deswelling, one should consider shrinking as a non-equilibrium process that depends on solvent transport. Once the gel is placed in the hot water bath, its surface temperature is first raised to above the LCST, thereby creating a temporary temperature gradient in the specimen, where the cool, swollen hydrogel core is covered by a hot, unswollen hydrogel layer. Since this layer (referred as the skin layer¹¹) is in its unswollen state, it possesses a higher crosslink density compared to the core, making it relatively stiff and less permeable to the solvent. As high temperatures advance towards the gel's center, the core undergoes phase transition, forcing it to expel water content towards the skin layer. This process is however constrained by the quasi-impermeability of the layer, forcing the core to remain at the swollen state with $J = J_s$ and subjecting the entire gel to a positive hydrostatic pressure P_g . As shown in Fig. 2e, this pressure may be relieved in two ways: first by fracturing the skin layer, or second by delamination between the skin and the hydrogel core. Our observations suggest that the second option occurs in heterogeneous manner, by nucleating numerous small blisters (Fig. 2e) that are able to grow as solvent flows from the core (Fig. 2f) to relieve its internal pressure. This situation is very similar to damage initiation in a variety of materials,^{38,39} where fracture nucleates from defects that are

randomly distributed throughout the material. Eventually, the entire gel specimen reaches its unswollen state as water slowly escapes by permeating through the inflated blisters.

The remainder of this paper concentrates on building a physical model describing the above processes and obtain general scaling laws for blister dynamics, sizes and concentration on the surface of deswelling hydrogels. Such laws will be an essential component in controlling the spatiotemporal morphology of hydrogel particles¹⁵ used in a variety of applications such as for biomedical devices¹⁸ and drug delivery systems.^{13,40}

3 MECHANICS OF BLISTER GROWTH ON A HYDROGEL SURFACE

Hydrogel surface blistering is characterized by the presence of two distinct length-scales associated with a single blister and the entire gel specimen, respectively. Our modeling approach follows this scale separation.

3.1 Blister mechanics and instability

To first understand the mechanism of the formation and growth of a single blister, we consider a surface defect laying near the surface of a small hydrogel volume V_g in its swollen state as shown in Fig. 3a. This defect is locally simplified as a cylindrical cavity

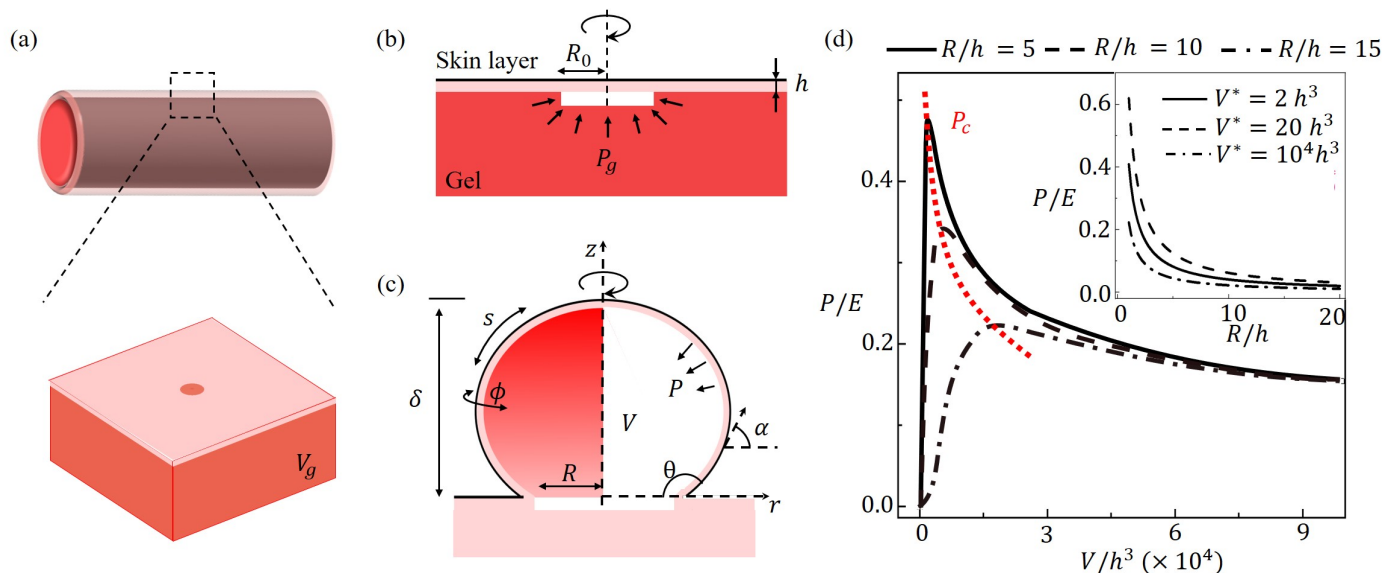


Fig. 3 (a) Schematic about the problem, we investigate the blistering on the surface of a cylindrical hydrogel. (b) Schematic about the cross section of the gel and the skin layer at the uninflated (reference) configuration. (c) The schematic of inflated configuration of the blister. (d) The internal pressure P is plotted as a function of the blister volume V and the neck radius R (inset).

of effective radius R_0 (Fig. 3b) located beneath a thin film (the skin layer) of thickness $h = 20\mu\text{m}$. This thickness is considered unchanged during the gel's volume phase transition as measured by Tokita et al.²⁷. Since the time for blister deflation (stage iv) is more than 3 times slower than the inflation process (stage i to iii), we assume that this film is impermeable. This implies that as the gel deswells and expels water, it is able to fill up the small defect, thereby raising the hydrostatic pressure P_g below the skin layer (Fig. 3b). This pressure, if large enough, may start the formation of a blister in two ways. First by inflating the thin film into a spherical shape, and second by triggering the delamination of the thin surface layer from the gel core.^{41,42} A model of these coupled phenomena was previously developed and we only highlight the key features in the present study. Readers are referred to Benet et al.⁴³ for more information on the formulation.

First, due to the small thickness of the skin layer compared to the typical blister size (around a millimeter in radius), it is modeled as a two-dimensional membrane, whose shape is defined by its mid-plane. Further using the axis-symmetry of a blister's shape, we describe its profile with the equation of a surface parameterized by the arclength $s(r, z)$ and azimuthal angle ϕ (as depicted in Fig. 3c) immersed in a three-dimensional space parameterized by the cylindrical coordinate system (r, ϕ, z) . The stretch of the membrane along the longitudinal (along the s -lines) and lateral (along ϕ -lines) can then be computed as $\lambda_s = ds/dr_0$ and $\lambda_\phi = r/r_0$ where r_0 is the radial coordinate of a point in its reference configuration, defined as the flat, unstretched circular membrane of radius R_0 (Fig. 3b). As the blister grows, the surrounding skin layer is stretched and the resulting tension applies a hydrostatic pressure P that resists blister inflation. The force equilibrium along the tangent and normal directions to the blis-

ter surface verifies:^{43,44}

$$\frac{d}{dr}(r\sigma_s) = \sigma_\phi \quad \text{and} \quad \frac{\sigma_s}{R_s} + \frac{\sigma_\phi}{R_\phi} = P \quad (2)$$

where σ_s and σ_ϕ are the line tensions along the longitudinal and lateral directions while $R_s = -\sqrt{1-(r')^2}/r''$ and $R_\phi = r/\sqrt{1-(r')^2}$ are the principal radii of curvature where $r' = dr/ds$.⁴⁴ Considering the skin layer as a neo-Hookean hyperelastic material, the line tensions can be related to the stretch ratios via the constitutive equations:^{44,45}

$$\sigma_s = \frac{Eh}{6} \left(\lambda_s^2 - \frac{1}{\lambda_s^2 \lambda_\phi^2} \right) \quad \text{and} \quad \sigma_\phi = \frac{Eh}{6} \left(\lambda_\phi^2 - \frac{1}{\lambda_s^2 \lambda_\phi^2} \right). \quad (3)$$

When occurring on a hydrogel surface, the growth of a blister depends on the competition between two antagonistic forces: the "forcing pressure P_g " exerted by the gel onto the skin layer.

For a given blister geometry – represented by its volume V and neck radius R (see Fig. 3c) – the internal pressure P can thus be determined by numerically solving the nonlinear equations eq. (2)-(3). Using this approach, we show in Fig. 3d the relationship between blister pressure and volume for a given neck radius R . It can be seen that when a blister is inflated at constant neck radius, its internal pressure P first increases monotonically until it reaches a critical (or maximum) value P_c , after which it decreases upon further inflation. This behavior is reminiscent of the mechanical instability that occurs during the inflation of rubber balloon⁴⁶ due to the geometrical instability of the thin rubber membrane. The model further predicts that a blister with larger neck radius exhibits a lower critical pressure but occurs at larger inflation volumes. Generally, as a blister grows, it can display both membrane stretch and delamination from its substrate. The delamination process is controlled by the energy release rate G , a measure of energy dissipation during the detachment of a unit

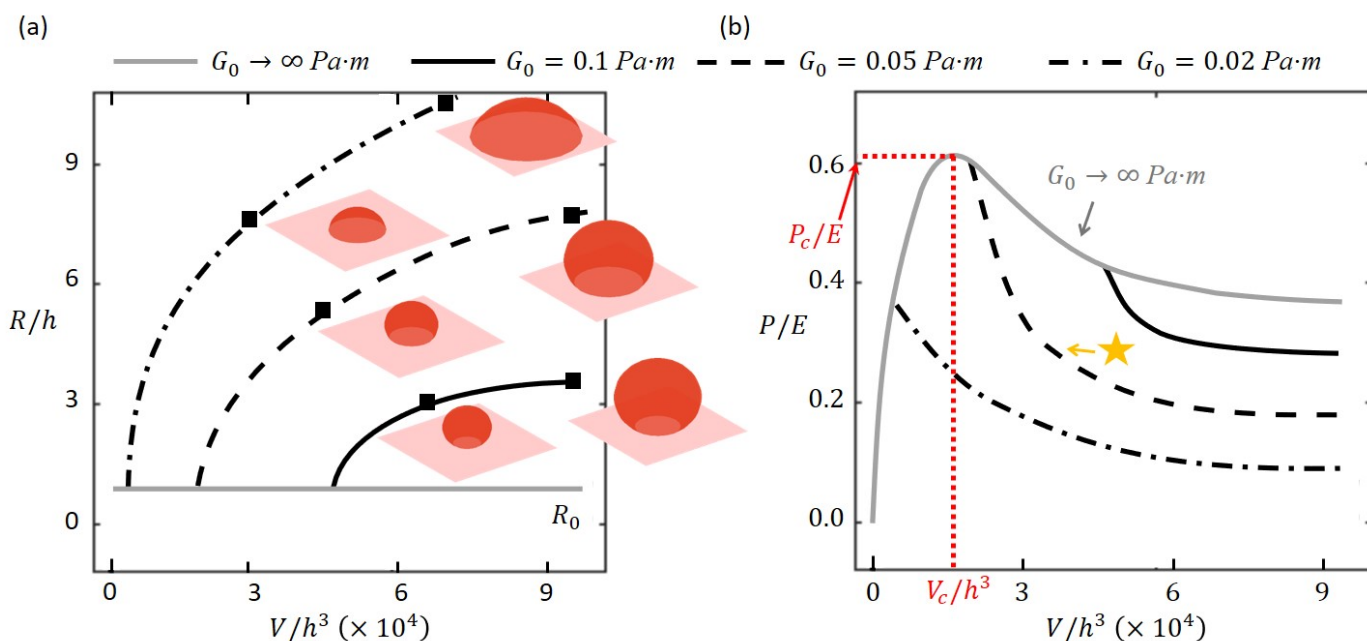


Fig. 4 (a) The change of blister radius during inflation for different values of G_0 . We also show two snapshots about the blister profile for each G_0 . (b) Pressure P as a function of V^* for different G_0 as the blister is inflated. In the following study, we will use the curve corresponding to $G_0 = 0.05$ for the $P - V^*$ relationship for a blister.

membrane area from the substrate. As shown by Benet et al,⁴⁷ and Long et al,⁴⁸ this quantity depends on the longitudinal stress σ_d^s and stretch λ_s at the neck in the form:

$$G = \sigma_d^s(\lambda_s - \cos\theta) - h\lambda_s\Delta\Psi_d^e \quad (4)$$

where $\Delta\Psi_d^e = E/6[\lambda_s^2 + \lambda_\phi^2 + 1/\lambda_s\lambda_\phi]^2 - 3$ is the stored elastic energy density per current volume at the neck, and θ is the contact angle of the blister on the gel. We note that the subscripts "d" in σ_d^s and $\Delta\Psi_d^e$ indicate quantities that are measured at the neck of the blister. The criterion for delamination can then be summarized as follows; when G is larger than the critical energy release rate G_0 , the mechanical energy provided to skin/gel boundary is large enough for decohesion and the neck radius grows. By contrast, as $G < G_0$, the neck radius remains constant and the blister grows by stretching its membrane in a quasi-spherical fashion. Fig. 4a shows model predictions of the inflation of blisters characterized by three different values of G_0 . The onset of delamination can be seen as the sudden increase of the neck radius from the initial value R_0 . We clearly see that for higher cohesion G_0 , delamination occurs at larger blister volumes and the blister takes a more spherical shape. Interestingly, we find that once delamination occurs, the equilibrium shape of a blister is fixed and solely depend on G_0 . This can be seen in Fig. 4a, where the shape of the blister remains unchanged during growth, but strongly depends on G_0 . Thus, for a small value of G_0 , one observes a flat, dome-shaped blister, while as G_0 increases, delamination is postponed and the blister converges to a spherical shape.

In summary, the growth of a blister of initial radius R_0 can be described by two stages. In the first stage, the blister grows at a constant neck radius R_0 until the energy release rate reaches

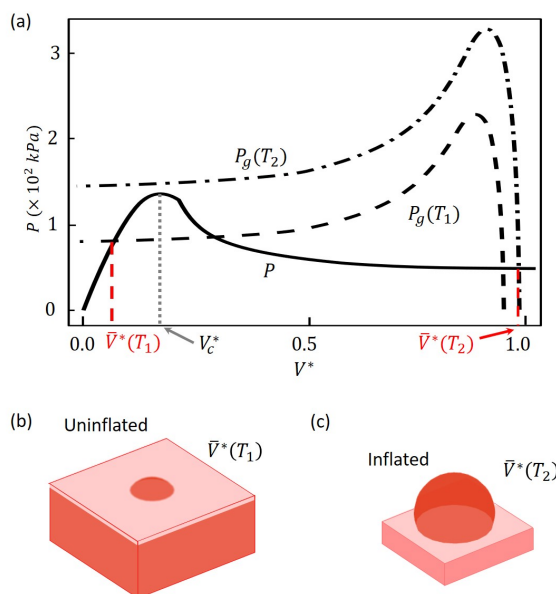


Fig. 5 (a) The forcing pressure P_g and the resisting pressure P as functions of relative volume V^* for different temperatures. (b) and (c) are the schematic illustration corresponding to $V^*(T_1)$ and $V^*(T_2)$.

the critical value ($G = G_0$). Once the critical energy release rate is reached, delamination occurs and the blister profile is entirely determined by G_0 . To further illustrate the effects of delamination on blister growth, we show the $P - V$ relationship for four blisters endowed with same initial radius R_0 but different values of G_0 . Again, the two growth stages can be observed: before delamination, the blister grows elastically and the curve displays the characteristic rubber instability at ($P = P_c$). After the onset

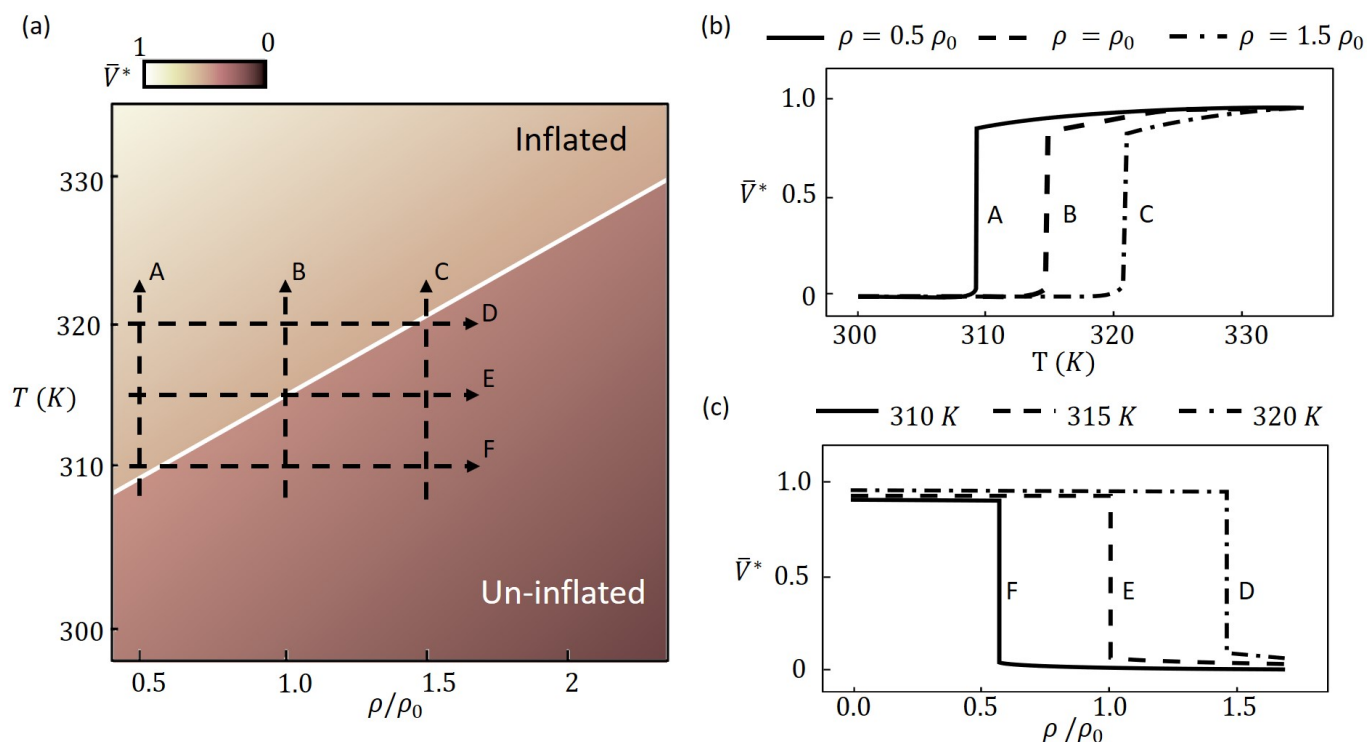


Fig. 6 (a) A phase diagram regarding the $V - \rho - T$ relationship. The phase boundary is obtained from eq.(6). The dash arrows correspond to the 6 different numerical cases about the effect of temperature on the blister volume (A-C) and the effect of crosslink density (D-F). (b) Blister volume as a functions of crosslink density ρ for three different temperatures. (c) Blister volume as a function of temperature T for three different crosslink densities.

of delamination, the growth in neck radius results in a sudden decrease in internal pressure, which is sustained as the blister grows. In the following study, the value $G_0 = 0.05 \text{ Pa} \cdot \text{m}$ (marked by a yellow star in Fig. 4b) is chosen as it leads to a similar blister profile to the equilibrium state observed experimentally (Fig. 1a and c).

3.2 Criterion for blister growth on a hydrogel surface

When occurring on a hydrogel surface, the growth of a blister depends on the competition between two antagonistic forces: the "forcing pressure P_g ", and the "resisting pressure P " resulting from skin tension around the blister. The driving force for blister growth may thus be defined as the difference $\Delta P = P_g - P$, such that $\Delta P > 0$ promotes growth while it vanishes when the blister is at equilibrium. The resisting pressure is obtained from Fig. 2b (we limit this study to the curve corresponding to $G_0 = 0.05 \text{ Pa} \cdot \text{m}$), while the forcing pressure is computed from eq.(1) and illustrated in Fig. 2b. Fig. 5a shows these competing pressures as a function of reduced blister volume $V^* = V/V_g$ (introduced in section 2) for two characteristic temperatures ($T_1 = 310 \text{ K}$ and $T_2 = 320 \text{ K}$). Interestingly, the equilibrium blister volume V^* can be graphically determined as the intersection of these two curves ($P_g = P$). At a lower temperature ($T = 310 \text{ K}$), equilibrium occurs at value of $V^* \approx 0.07$, which corresponds to a nearly flat (or unflated) blister with the majority of the solvent remaining in the gel (Fig. 5b). As temperature increases however ($T = 320 \text{ K}$), the forcing pressure becomes larger and the equilibrium is found at $V^* \approx 0.93$, corresponding to the inflation of a large dome-shaped blister on a dry

hydrogel body (Fig. 5c). In this case, the blister is considered inflated.

Fig. 5a shows that blister inflation only occurs if the forcing pressure is sufficiently large so that it triggers the mechanical instability. This condition can be evaluated by comparing the magnitudes P_c and P_{gc} of the forcing and resisting pressures at the critical volume V_c^* at which instability happens. If the forcing pressure is larger at $V^* = V_c^*$, the instability is triggered and the blister is inflated. Otherwise the blister remains uninflated. The state of a blister may thus be predicted by the relative magnitudes of P_c and P_{gc} at V_c^* . For this, let us define β as the ratio of these two pressures as $\beta = P_{gc}/P_c$. With this definition, a boundary between the inflated and uninflated state of a blister can then be found as $\beta = 1$, such that the instability is triggered and the blister is inflated when $\beta > 1$.

3.3 Effect of crosslink density and temperature on blister inflation

To further understand the role of hydrogel structure and temperature on the appearance of blisters, let us consider how these two factors regulate the competition between the resisting pressure and forcing pressure. First, the resisting pressure P_c is associated to crosslink density and temperature via the Young's modulus $E = 3\rho k_B T$. According to Fig. 4b, the resisting pressure can be computed by $P_c = 3\rho k_B T f(V_c^*)$ where $f(V_c^*)$ is a constant (obtained numerically from eq.(2)-(4)) determined by the critical reduced volume for instability. Regarding the forcing pressure P_{gc} , its dependency on crosslink density and tem-

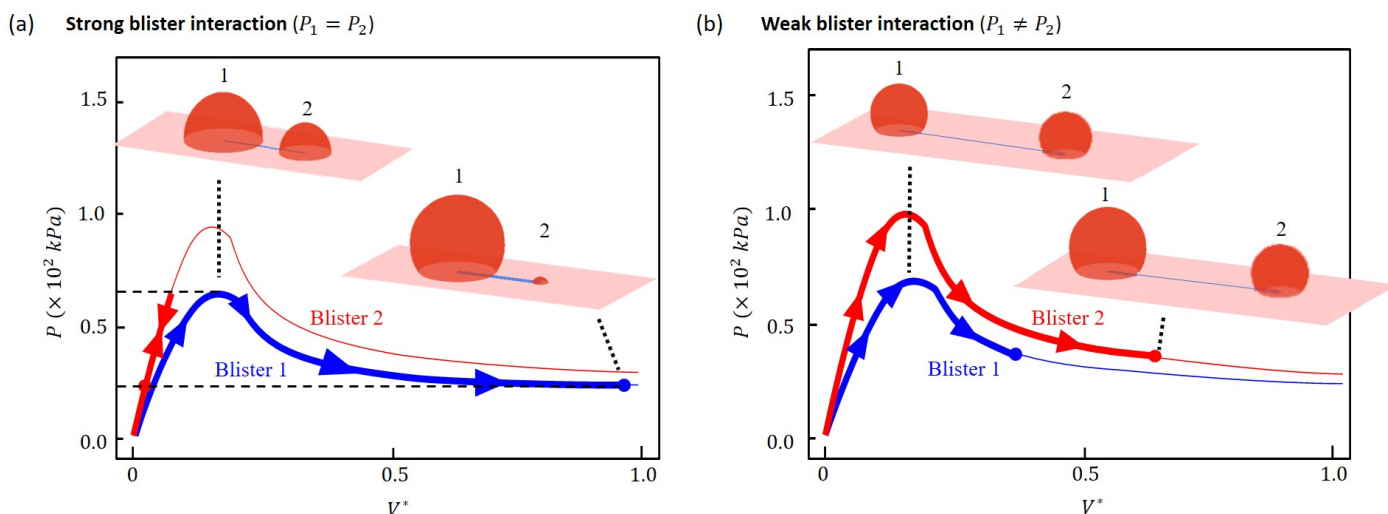


Fig. 7 Example of the $P - V$ paths of two neighboring blisters when (a) the blister interaction is strong; and (b) the blister interaction is weak.

perature is less obvious since it is the sum of two contributions: the elasticity of the network and the osmotic pressure, as shown in eq. (1). For this, we note that eq. (1) can be rewritten as $P_{gc} = k_B T [3g(J_c)\rho + \pi_0(J_c)T + \pi_1(J_c)]$, where $g(J_c)$ is the constant associated with the elastic pressure of hydrogel, while $\pi_0(J_c)$ and $\pi_1(J_c)$ are associated with the osmotic pressure. In addition, the variable J_c is the swelling ratio of the gel at $V^* = V_c^*$ computed by $J_c = (1 - V_c^*) / (1 - V_0^*)$ where V_0^* is the reduced volume of dry hydrogel. The forms of g , π_0 and π_1 are found as $g(J_c) = 1/J_c^{1/3} - 1/J_c$, $\pi_0(J_c) = \chi_1/vJ_c^2$ and $\pi_1(J_c) = [\ln(1 - 1/J_c) + 1/J_c + A_0/J_c^2]$. Using the above information, the ratio β can be computed in terms of ρ and T as:

$$\beta = \frac{P_{gc}}{P_c} = \beta_0 + \frac{\beta_1}{\rho} + \frac{\beta_2 T}{\rho} \quad (5)$$

where $\beta_0 = g/f$, $\beta_1 = \pi_1/f$ and $\beta_2 = \pi_0/f$. We see that β is inversely proportional to ρ and linearly proportional to T . This indicates that the blister inflation is promoted by an increase in temperature but hindered by an increase in crosslink density. In the crosslink density ρ - temperature T space, the boundary between the inflated and uninflated state of a blister can be found by $\beta = 1$, which is represented by a linear relationship:

$$T = \frac{T(1 - \beta_0)}{\beta_2} - \frac{\beta_1}{\beta_2} \quad (6)$$

This equation can be graphically represented by the phase diagram of Fig. 6a, showing the boundary between inflated and uninflated states. To confirm the above analysis, we then performed a parametric study of the equilibrium blister using the numerical methodology discussed in section 3.2. As expected, Fig. 6b shows a clear transition from the inflated to the uninflated state when the crosslink density is increased or when temperature decreases below the LCST (Fig. 6 b and c).

4 GROWTH OF MULTIPLE BLISTERS

The heterogeneous blister inflation on gel surfaces observed experimentally^{24,26,29} (Fig.1a and c) suggests that surface blisters do not grow individually, but tend to interact with their close neighbors. To explore this collective behavior, we now extend our model to the case of multiple blisters with the objective to explain the variety of surface profiles shown in Fig. 1.

4.1 Interaction between blisters during growth

To understand blister-blister communication, let us first consider two neighboring blisters whose pressure can be locally mediated by solvent transport. Fig. 7 illustrates this interaction by showing the inflation and internal pressure of two adjacent blisters whose P-V relationships slightly differ due to small heterogeneities in defect size and geometry. To differentiate the two blisters, we use red curves to plot the P-V relation of blister 1 (left) and blue curves for blister 2 (right). The inflation paths of these two blisters are shown by thick lines along their $P - V$ curves, where arrows show whether the blister is inflating (arrow towards $V^* = 1$) or deflating (arrow towards $V^* = 0$). The equilibrium state is shown by circular marks. In this illustration, the blisters' interaction is controlled by varying their separation distance. When the blisters are near each other (Fig.7a), the solvent can quickly be transported across the gel and the pressure equilibration is quasi-instantaneous. As a result, when the blister with the lowest critical pressure becomes unstable, its pressure decreases upon inflation. To accommodate this pressure drop, the second blister (which has not passed its critical pressure), is forced to reduce its pressure by reducing its volume and flattens out. This scenario eventually leads to the inflation of a single blister at the detriment of its neighbor. Alternatively, one can consider a situation in which two blisters are far enough so that local pressure field to not influence one-another (Fig. 7b). In this case, solvent transport across blisters is insignificant and the blisters grow independently into two smaller blisters (since the volume of expelled water is divided between the

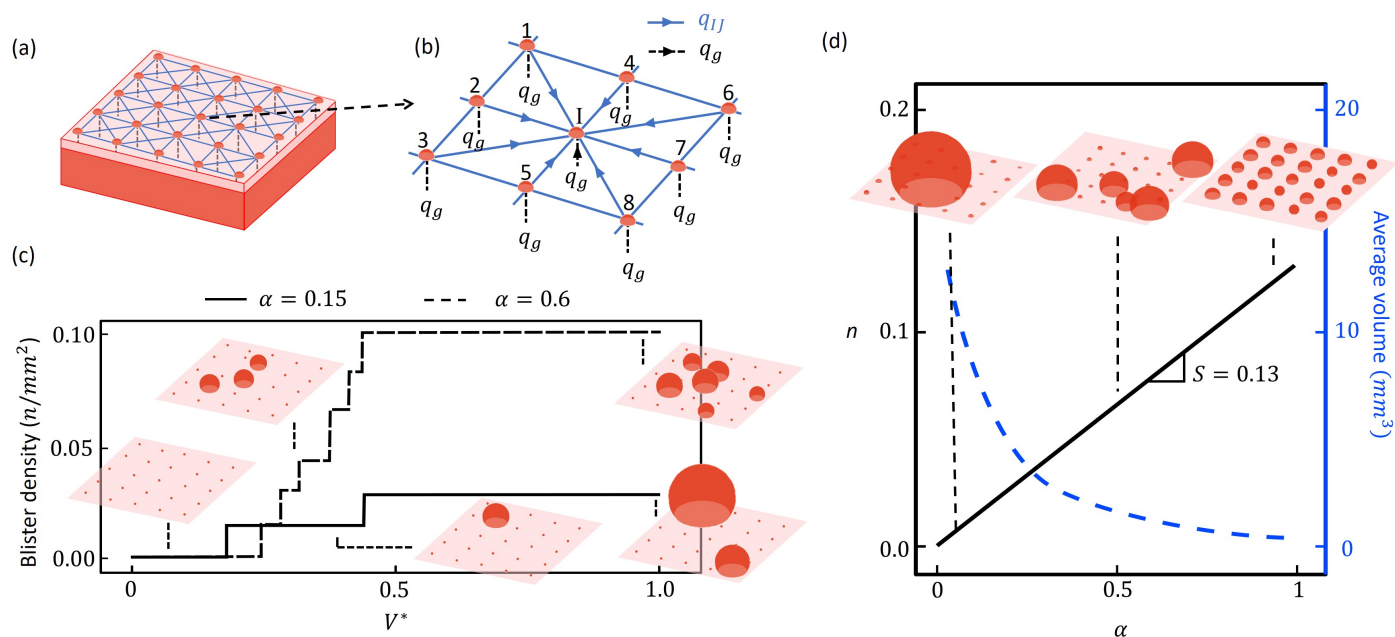


Fig. 8 (a) Schematic of the stochastic model where a hydrogel surface is considered to contain a lattice of $N \times N$ defects. Here, we show the portion of 6×6 as an example. (b) Schematic illustration about how one blister site (labeled by I) is connected to the neighboring blisters (labeled by 1-8) and the gel. The solvent transport between the blisters is measured by q_{IJ} and the transport between the gel and the blister is measured by q_G . (c) The change of blister density during the inflation history when $\alpha = 0.5$ and 0.2 . (d) The density and average volume of blisters as a function of α .

two of them). The above two examples represent two extreme cases of what may happen in experimental conditions. Indeed, solvent transport across neighboring blister will vary with hydrogel cross-link density, defect distributions and temperature. Furthermore, blister interactions usually occur between more than two blisters, leading more complex situations as observed in Fig.1. We next assess these mechanisms using a numerical model.

Modeling: We developed a stochastic model of several inflating blisters, interacting via the redistribution of solvent flow. In this model, blisters inflation was simulated on a square domain of edge length 5 cm , similar to the length of hydrogels used in experiment. This domain is considered to contain a lattice of $N \times N$ defects (Fig. 8a shows an example of a small portion of 6×6 defects) by computing the solvent flux q at each site according to the following approach. First, solvent transport through the gel was assessed by modeling the hydrogel as a network of segments linking each defect site to the gel core (vertical segments) and to neighboring defects (horizontal segments). For clarity, let us consider a particular blister site (labeled by index I), that possesses 8 neighboring blisters (Fig. 8b), labeled $J = 1 - 8$. A blister is therefore connected to 9 segments, 8 of which are associated with a solvent influx q_{IJ} arising from blister-blisters interactions, and 1 of them associated with the influx q_G , arising from gel-blisters interactions. Using Darcy's law,⁴⁹ the solvent transport can be written in terms of pressure gradient between blisters and hydrogel's apparent permeability κ such that:

$$q_I = \sum_{J=1}^8 q_{IJ} + q_G \quad q_{IJ} = \frac{\kappa(P_J - P_I)}{\ell} \quad (7)$$

where ℓ is the average distance between defects and the term $(P_J - P_I)/\ell$ is the average pressure gradient between defects. A positive flux q_{IJ} indicates solvent transport from defect site J to I . The apparent permeability κ has a unit of $m^5 \cdot s/kg$ and is related to the commonly used hydrodynamic permeability κ_h through $\kappa_h = \kappa\mu/A$ where μ is the dynamic viscosity of solvent and A is the cross section area across which solvent transport takes place (e.g., a thin region beneath the skin layer). Knowing the flux q_I , the volume and pressure in blister I could then be determined by integrating its inflation rate over time ($V_I = \int_0^t q_I dt$) and using the pressure-volume relationship $P_I = P_I(V_I)$ determined from eq. (2)-(4) (shown in Fig. 5b). The reduced volume of the gel is computed by $V^* = 1 - (\sum_{I=1}^n V_I)/V_s$ where V_s is the initial volume the gel at swollen state. These equations are solved incrementally using a Backward-Euler integration scheme that allows us to follow the volume and pressure evolution of each blister over time. Square lattices with 20×20 sites were used for our simulations, all subjected to periodic boundary conditions on the edge of the square domain to avoid boundary effects. We found that this number of lattice sites was sufficient to obtain converging results, i.e. further increasing the number of lattice sites only increased the computational cost without affecting the results. Importantly, to account for the structural heterogeneity of the gel, the defect's radii were assumed to follow a normal distribution around an average value R_0 (with a standard deviation of $0.1 R_0$), which introduced minute differences in the initial stiffness and critical pressure of individual blisters. Due to the stochasticity in the blister geometry, the computational results are generated by averaging 20 simulations produced with the same material parameters.

Results and interpretation Before presenting numerical results, it is first important to note that interactions between neighboring blisters is mediated by two competing time scales: the time τ_g to inflate a blister and the time τ required to transport solvent between a blister to its neighbors. Using the fact that these time scales are inversely proportional to flux, we can write $\tau \propto 1/|q|$. Further noting that the pressure difference $P_j - P_l$ between two blisters is on the order of the critical blister pressure P_c , the two competing time scales are defined as $\tau \propto l/(\kappa P_c)$ and $\tau_g \propto 1/q_G$. To further reduce the problem, we note that the competition between blisters depends on the ratio of the characteristic times, i.e.,

$$\alpha = \frac{\tau}{\tau_g} = \frac{q_G \ell}{\kappa P_c}. \quad (8)$$

In other words, when $\alpha \rightarrow 0$, the time for blister interaction is much shorter than the inflation time and the pressures between two adjacent blisters immediately equilibrate as seen in Fig. 7a. As α increases, the interaction time becomes longer, and the competition eventually switches to the second case illustrated in Fig. 7b. As shown in eq. (8), this competition can be regulated by either varying the inter-blisters distance ℓ , the apparent permeability κ , the blister properties, or the influx q_G . The latter was chosen, as the former quantities are not easily manipulated experimentally. For this, we set $\kappa = 1 \text{ m}^5 \cdot \text{s}/\text{kg}$ and chose $\ell = 500 \text{ }\mu\text{m}$. Considering that the hydrogel sample is a few centimeters in size, this characterizes a large defect density. We note that the value of these two parameters are manually set to gain a qualitative understanding of the competition and do not represent the properties of actual hydrogel. Fig. 8c shows the inflation of multiple blisters for $\alpha = 1/2$ and $\alpha = 2$, where the blister density n is plotted as a function of the reduced volume V^* . We clearly see here that a larger α promotes the inflation of more numerous and smaller blisters. Indeed, a large α implies that the time for blister interaction is slow; which drives them to grow and reach their instability point independently. As a result, when $\alpha = 3$, we see a blister is initiated at each defect site. Fig. 8d depicts how the parameter α affect the final blister density and indicates that blister density scales linearly with α in the form $n = S\alpha$ where S measures the sensitivity of n to α . We found that $S = 0.13/\text{mm}^2$ according to the results of Fig.8b.

Since inflated blisters collectively share the water expelled by the gel, the average volume of inflated blisters is inverse proportional with α .

Dependency of hydrogel blistering on crosslink density and temperature To relate the results of Fig. 8d to the gel crosslink density and temperature, let us now relate the flux q_{GI} to the mechanics of gel deswelling discussed earlier. For this, for a particular blister site (labeled by index I), the influx q_{GI} is computed by the Darcy's law as:

$$q_{GI} = \frac{\kappa(P_G - P_I)}{\ell_c} \quad (9)$$

where P_g is the deswelling pressure in the gel computed from eq. (1) and P_l is the resisting pressure obtained from Fig. 5b and

$\ell_c = (V_c)^{1/3}$ is characteristic length scale associated with a single blister. Scaling-wise, the gel pressure P_g is on the order of P_{gc} , while P_l is on the order of P_c . Using eq. (5), we can therefore deduce that $q_{GI} \approx \kappa(\beta - 1)P_c/\ell_c$. In other words, the competition parameter becomes:

$$\alpha = (\beta - 1) \frac{\ell}{\ell_c} \quad (10)$$

Using eq. (5), it is then straightforward to find that α is inversely proportional to cross-link density and linearly dependent on temperature. Further using the linear relationship between blister density and α ($n = S\alpha$ from Fig.8d) one can then directly predict how n depends on ρ and T . Using eq. (5) and eq.(10), we can then find:

$$n = S \frac{\ell}{\ell_c} \left[\beta_0 - 1 + \frac{\beta_1 + \beta_2 T}{\rho} \right] \quad (11)$$

where β_0 , β_1 and β_2 are constants shown in eq. (5) associated to the forcing pressure and the resisting pressure for blister inflation. This relationship is reported in Fig.9 and compared with experimental results.

A parametric study, whose results are reported Fig. 9a indeed confirms this analysis. We further observe that above a critical crosslink density; blisters do not appear since the forcing pressure becomes insufficient to inflate the blisters (see section 3.3). For different temperatures, this critical crosslink density can be found from the phase diagram of Fig. 6c. Finally, Fig. 9b shows our simulation results of the hydrogel's surface profile for six different $\rho - T$ combinations (the hydrogel surface is wrapped into a cylinder for visualization purpose). We see that both a larger ρ (A-C) and lower T (C-E) lead to a decrease in blister density. In the extreme situation (F), only one large blister is observed on the gel surface. The model predictions qualitatively match experimental results in terms of blister density and size. In fact, by choosing the value $\ell/\ell_c = 0.79$, we obtain a satisfactory match between modeling results (showed by solid lines) and experimental measurements (replicated from Fig. 1b and plotted by symbols). At low crosslink density ($\rho = 0.54\rho_0$), the model slightly overpredicts the blister density, an error that is attributed to the impermeability assumption for the skin layer. Indeed, at low crosslink density, the blister growth is most likely hindered by solvent leak through the gel's surface.

5 CONCLUSION

As a summary, we have experimentally and theoretically studied the surface blistering of PNIPAm hydrogel during its volume phase transition. Mechanically, we found that the inflation of a single blister depends on two competing pressures, namely, the "forcing pressure" – that originates from hydrogel deswelling and promotes inflation – and the "resisting pressure" – that arises from the elasticity of the blister and inhibits inflation –. The interplay between these two pressure can be adjusted by varying crosslink density and temperature. Importantly, as it grows, a blister goes through a mechanical instability after which inflation continues without a rise in forcing pressure. An outcome of this response is that multiple blisters are able to "communicate" with one-another via fluid pressure as they grow. Indeed, once a blister

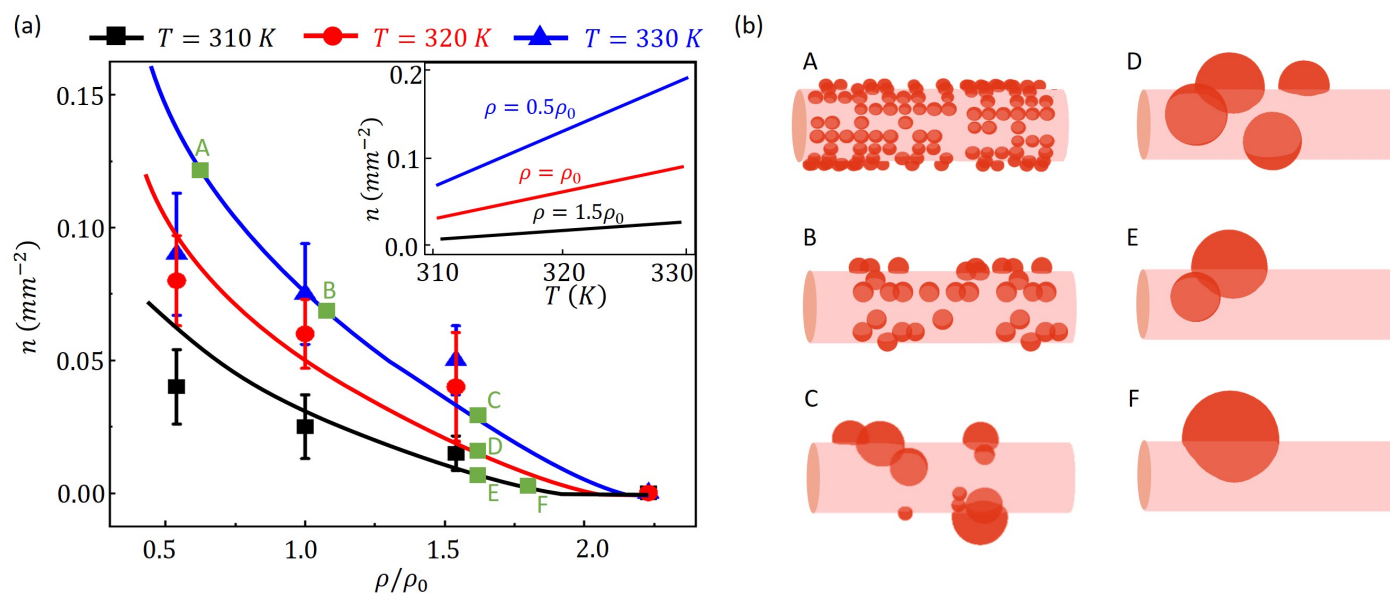


Fig. 9 (a) Blister density as a function of crosslink density and temperature: comparison between computational model (solid lines) and experiments (discrete symbols and error bars). Each experimental data point is collected from 3 repetitions. (b) Predicted hydrogel profile for different crosslink densities and temperatures (each condition is labelled by the green blocks in (a) with index A-F). The surface was wrapped in a cylindrical shape for better comparisons with experimental data of Fig. 1b.

has gone through its instability, it grows without resistance and sucks-in the solvent from its closest neighbors, thereby stopping their growth. Our analysis shows that this competition between neighbors is governed by the ratio α between two time scales: the time for blister inflation and the time for blister interaction. A simple computational model of these interactions shows a linear relationship between α and the density of fully grown blisters on the gel surface. By the qualitative matching between experimental and modeling results, this model also unveils the dependency of surface blistering profile on the crosslink density and temperature. This phenomenon is reminiscent of phase separation/ pattern formation arising from activator-inhibitor systems. Surface blisters on PNIPAM hydrogel indeed possess the two main components enabling pattern formation. First, the presence of a "self-enhancing" mechanisms enabled by the mechanical instability of growing blisters. This instability indeed enables a blister to sustain unlimited growth with very little driving pressure. Second, the "long-range inhibition" mechanism due to the fact that a fast growing blister consumes most of the solvent in its vicinity, thereby depleting additional resources from its neighbors. Interestingly, in contrast with classical activator-inhibitor models based on Turing's chemical reactions,⁵⁰ blisters rely on unstable growth and solvent transport, whose relative rates drives the pattern formation. Cell blebbing⁷ and other biological processes may rely on this interplay between mechanics and transport.

Being able to temporally and spatially control the surface blistering process will open the door to the development of a synthetic system that closely mimics the various blebbing behaviors of cells (e.g., apoptosis and blebbing-based locomotion). Such synthetic system may also enhance our understanding of

biological processes behind the mechanical behavior of cells by accurately controlling their environment. From an engineering perspective, this is also of interest to many applications, especially for hydrogel-based drug delivery systems.³⁰ In order to achieve this, a high fidelity modeling framework is needed to accurately predict the spatial and temporal blistering profile of hydrogel. We note that the current single blister model is developed based on several simplifying assumptions: the axisymmetry of the blister's shape, the non-deformability of the core and the impermeability of the skin layer. However, several experimental observations indicate that these assumptions are not always satisfied. For instance, blisters may evolve non-axisymmetrically due to the curved gel surface, the gel's core bends due to the anti-symmetric blistering and the inflated blisters slowly deflate and eventually vanish. Future efforts that relax these could predict more complicated inflation behaviors as well as blister-gel interactions (e.g., blistering-induce bending of the gel). In addition, blisters may cause damage of the hydrogel network in both the skin layer and in the gel's core.⁵¹ Its effect on the mechanical response needs to be evaluated when considering problems involving cyclic pattern formation. Regarding multiple blisters interaction, higher fidelity models are also needed to quantitatively capture the solvent transport that originate from blister-blisters interaction and the gel-blisters interaction.^{52,53}

Acknowledgements. Research reported in this publication was supported by the National Science Foundation under the award 1761918. The content is solely the responsibility of the authors and does not necessarily represent the official views of the National Science Foundation.

References

- 1 A. Juel, D. Pihler-Puzovic and M. Heil, *Annual Review of Fluid Mechanics*, 2018, **50**, 691–714.
- 2 C. Sitaru and D. Zillikens, *Experimental Dermatology*, 2005, **14**, 861–875.
- 3 W. Funke, *Progress in Organic Coatings*, 1981, **9**, 29–46.
- 4 A. D. Adamczak, A. A. Spriggs, D. M. Fitch, C. Burke, E. E. Shin and J. C. Grunlan, *Polymer Composites*, 2011, **32**, 185–192.
- 5 L. Casciola-Rosen, A. Rosen, M. Petri and M. Schlissel, *Proceedings of the National Academy of Sciences*, 1996, **93**, 1624–1629.
- 6 B. Maugis, J. Bruguères, P. Nassoy, N. Guillen, P. Sens and F. Amblard, *Journal of Cell Science*, 2010, jcs.065672.
- 7 E. K. Paluch and E. Raz, *Current Opinion in Cell Biology*, 2013, **25**, 582–590.
- 8 G. T. Charras, *Journal of Microscopy*, 2008, **231**, 466–478.
- 9 M. C. Koetting, J. T. Peters, S. D. Steichen and N. A. Peppas, *Materials science & engineering. R, Reports : a review journal*, 2015, **93**, 1–49.
- 10 Y. Hirokawa and T. Tanaka, *AIP Conference Proceedings*, 1984, **107**, 203–208.
- 11 E. Sato Matsuo and T. Tanaka, *The Journal of Chemical Physics*, 1988, **89**, 1695–1703.
- 12 A. Suzuki and T. Ishii, *The Journal of Chemical Physics*, 1999, **110**, 2289–2296.
- 13 S. Purushotham, P. E. J. Chang, H. Rumpel, I. H. C. Kee, R. T. H. Ng, P. K. H. Chow, C. K. Tan and R. V. Ramanujan, *Nanotechnology*, 2009, **20**, 305101.
- 14 N. S. Satarkar and J. Z. Hilt, *Journal of Controlled Release*, 2008, **130**, 246–251.
- 15 M. Onoda, T. Ueki, R. Tamate, M. Shibayama and R. Yoshida, *Nature Communications*, 2017, **8**, 15862.
- 16 T. Shen, M. G. Font, S. Jung, M. L. Gabriel, M. P. Stoykovich and F. J. Vernerey, *Scientific reports*, 2017, **7**, 16178.
- 17 F. Vernerey and T. Shen, *Journal of The Royal Society Interface*, 2017, **14**, 20170242.
- 18 C.-H. Zhu, Y. Lu, J. Peng, J.-F. Chen and S.-H. Yu, *Advanced Functional Materials*, 2012, **22**, 4017–4022.
- 19 A. Richter, S. Howitz, D. Kuckling and K.-F. Arndt, *Sensors and Actuators B: Chemical*, 2004, **99**, 451–458.
- 20 T. Tanaka, *Physica A: Statistical Mechanics and its Applications*, 1986, **140**, 261–268.
- 21 G. Bai and A. Suzuki, *The Journal of Chemical Physics*, 1999, **111**, 10338–10346.
- 22 G. Bai and A. Suzuki, *Materials & Design*, 2000, **21**, 547–550.
- 23 T. Tanaka, *Polyelectrolyte Gels*, American Chemical Society, 1992, vol. 480, pp. 1–21.
- 24 T. Okajima, I. Harada, K. Nishio and S. Hirotsu, *The Journal of Chemical Physics*, 2002, **116**, 9068–9077.
- 25 S.-i. Takata, K. Suzuki, T. Norisuye and M. Shibayama, *Polymer*, 2002, **43**, 3101–3107.
- 26 S. Dutta and D. Dhara, *Polymer*, 2015, **76**, 62–69.
- 27 M. Tokita, S. Suzuki, K. Miyamoto and T. Komai, *Journal of the Physical Society of Japan*, 1999, **68**, 330–333.
- 28 M. Tokita, K. Miyamoto and T. Komai, *The Journal of Chemical Physics*, 2000, **113**, 1647–1650.
- 29 M. Shibayama and K. Nagai, *Macromolecules*, 1999, **32**, 7461–7468.
- 30 Y. Kaneko, R. Yoshida, K. Sakai, Y. Sakurai and T. Okano, *Journal of Membrane Science*, 1995, **101**, 13–22.
- 31 J. Dervaux and M. B. Amar, *Annual Review of Condensed Matter Physics*, 2012, **3**, 311–332.
- 32 F. Afroze, E. Nies and H. Berghmans, *Journal of Molecular Structure*, 2000, **554**, 55–68.
- 33 E. M. Ahmed, *Journal of advanced research*, 2015, **6**, 105–121.
- 34 P. Flory *et al.*, NY: Cornell University, 1953.
- 35 K. I. MacConaghy, D. M. Chadly, M. P. Stoykovich and J. L. Kaar, *Analytical chemistry*, 2015, **87**, 3467–3475.
- 36 G. A. Holzapfel, *Meccanica*, 2002, **37**, 489–490.
- 37 S. Cai and Z. Suo, *Journal of the Mechanics and Physics of Solids*, 2011, **59**, 2259–2278.
- 38 A. N. Gent and D. A. Tompkins, *Journal of Applied Physics*, 1969, **40**, 2520–2525.
- 39 V. Lefèvre, K. Ravi-Chandar and O. Lopez-Pamies, *International Journal of Fracture*, 2015, **192**, 1–23.
- 40 N. S. Satarkar and J. Z. Hilt, *Acta biomaterialia*, 2008, **4**, 11–16.
- 41 J. Chopin, D. Vella and A. Boudaoud, *Proceedings of the Royal Society of London A: Mathematical, Physical and Engineering Sciences*, 2008, **464**, 2887–2906.
- 42 H. M. Jensen, *Engineering Fracture Mechanics*, 1991, **40**, 475–486.
- 43 F. V. Eduard Benet, Hongtian Zhu, *Physical Review E*, 2019.
- 44 R. Long and C.-Y. Hui, *International Journal of Solids and Structures*, 2012, **49**, 672–683.
- 45 R. Long and C.-Y. Hui, *International Journal of Solids and Structures*, 2012, **49**, 672–683.
- 46 J. A. Zimmerman and A. J. Crosby, *Journal of Polymer Science Part B: Polymer Physics*, 2010, **48**, 1423–1427.
- 47 E. Benet and F. Vernerey, *Soft Matter*, Submitted.
- 48 R. Long, K. R. Shull and C.-Y. Hui, *Journal of the Mechanics and Physics of Solids*, 2010, **58**, 1225–1242.
- 49 S. Whitaker, *Transport in porous media*, 1986, **1**, 3–25.
- 50 S. Kondo and T. Miura, *science*, 2010, **329**, 1616–1620.
- 51 F. J. Vernerey, R. Brighenti, R. Long and T. Shen, *Macromolecules*, 2018, **51**, 6609–6622.
- 52 V. Dhote and F. J. Vernerey, *Biomechanics and modeling in mechanobiology*, 2014, **13**, 167–183.
- 53 U. Akalp, S. J. Bryant and F. J. Vernerey, *Soft Matter*, 2016, **12**, 7505–7520.